

VA-Adapter: Adapting Ultrasound Foundation Model to Echocardiography Probe Guidance

Teng Wang^{1,*}, Haojun Jiang^{1,*}, Yuxuan Wang², Zhenguo Sun³, Yujiao Deng⁴, Shiji Song¹ and Gao Huang^{1,†}

Abstract—Echocardiography is a critical tool for detecting heart diseases, yet its steep operational difficulty causes a shortage of skilled personnel. Probe guidance systems, which assist in acquiring high-quality images, offer a promising solution to lower this operational barrier. However, robust probe guidance remains challenging due to significant individual variability. This variability manifests as differences in low-level features within two-dimensional (2D) images, which complicates image feature understanding, and differences in individual three-dimensional (3D) structures, which poses challenges for precise navigation. To address these challenges, we first propose leveraging the robust image representations learned by ultrasound foundation models from vast datasets. Yet, applying these models to probe navigation is non-trivial due to their lack of understanding of individual 3D structures. To this end, we meticulously design a Vision-Action Adapter (VA-Adapter) to online inject the capability of understanding individual 3D structures. Specifically, by embedding the VA-Adapter into the foundation model’s image encoder, the model can infer cardiac anatomy from historical vision-action sequences, mimicking the cognitive process of a sonographer. Extensive experiments on a dataset with over 1.31M samples demonstrate that the VA-Adapter outperforms strong probe guidance models while requiring approximately 33 times fewer trained parameters.

Index Terms—echocardiography, adapter, sequence modeling, probe guidance, foundation model.

I. INTRODUCTION

Cardiovascular diseases have become a significant factor affecting human lifespan [25]. Echocardiography is a commonly used imaging technique for diagnosing cardiovascular diseases, allowing the observation of the health conditions of heart chambers, valves, and blood vessels [21]. With technological advancements, AI-driven echocardiography diagnostic models [6], [8], [24] have demonstrated remarkable capabilities. As shown in Fig. 1(a), representative models in this domain include EchoCLIP [6], a foundation model pre-trained on a dataset of over a million paired cardiac ultrasound videos and expert reports; USFM [17], which is pre-trained on over two million ultrasound images covering 12 different organs; and BiomedCLIP [32], which is pre-trained on 15.3 million image–text pairs extracted from 4.4 million articles in PubMed. All three models demonstrate strong capabilities in interpreting cardiac ultrasound images.

This work is supported by Ministry of Industry and Information Technology of the People’s Republic of China (2024YFB4708200).

¹Department of Automation, BNRist, Tsinghua University, Beijing, China. ²School of Computer Science and Technology, Xidian University, Xi’an, China. ³Beijing Academy of Artificial Intelligence, Beijing, China. ⁴Department of Ultrasound, The First Medical Center of Chinese PLA General Hospital, Beijing, China.

*These authors contributed equally to this work.

§Haojun Jiang guided this work.

†Corresponding author: Gao Huang. Email: gaohuang@tsinghua.edu.cn

Undoubtedly, the prerequisite for these powerful diagnostic models to function effectively is the availability of high-quality ultrasound images. However, due to the inherently high operational difficulty of cardiac ultrasound, it takes years of training for a beginner to master the technique, resulting in a scarcity of skilled professionals. Therefore, leveraging AI technology to assist in cardiac ultrasound scanning is a crucial research direction.

In recent years, researchers [1], [3], [7], [13]–[16], [18], [22], [28] have proposed developing AI-driven probe guidance systems to provide junior sonographers with recommendations for probe adjustment actions, aiming to acquire higher-quality ultrasound images. For example, Droste et al. [7] proposed a model named US-GuideNet to guide the scanning of fetal planes. Later, Narang et al. [22] collected a vast amount of echocardiography scanning data and trained a convolutional neural network-based guidance system from scratch. However, the system is intended for commercial use, and its technical implementation details are closed-source. Li et al. [18] proposed utilizing cardiac CT data as a simulation environment and employing reinforcement learning to train guidance strategies. While these works achieved progress, they studied probe guidance separately from diagnosis, without leveraging advancements in diagnostic models [6], [17], [31], [32], *e.g.*, EchoCLIP. Both scanning and diagnosis require models to understand structures in cardiac ultrasound images and make decisions, leading us to hypothesize that advancements in diagnostic models can also enhance probe guidance models.

In this paper, we aim to build upon the ultrasound foundation model’s ability to interpret cardiac ultrasound images by equipping it with the capability to understand three-dimensional cardiac structures and reason about probe adjustment actions. First, to preserve the basic capabilities learned by foundation model from large-scale data as much as possible, we employ a parameter-efficient fine-tuning strategy called Adapter, which freezes the foundation model’s image encoder and only optimizes the parameters within the adapter. Meanwhile, we observe that sonographers in practice often leverage information from past explorations, including image and action sequences, to optimize their decision-making. Inspired by this, we meticulously design a Vision-Action Adapter (VA-Adapter) to process sequential information and learn about the three-dimensional structure of the heart from it. Specifically, VA-Adapters are inserted into the deeper layers of the image encoder of foundation model, as the features in the shallow layers are typically more general, while the features in the deeper layers are usually more task-relevant [29]. Finally, extensive experiments demonstrate that the VA-Adapter equips

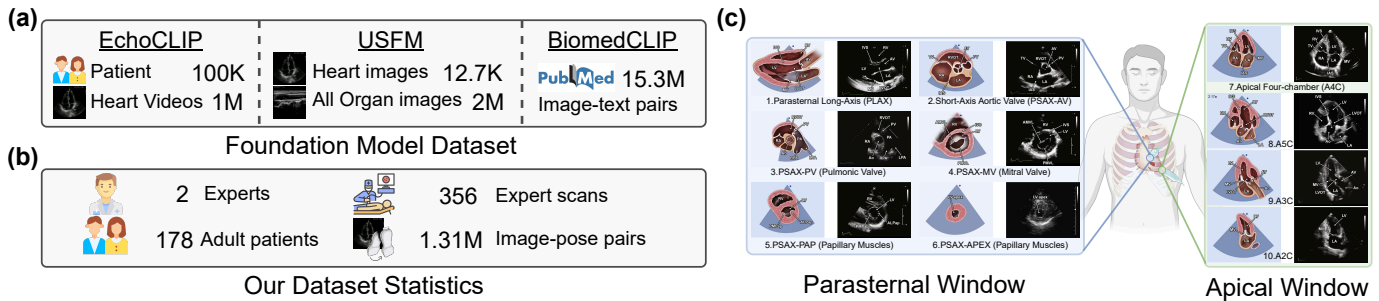


Fig. 1: Illustration of the dataset. (a) Large-scale diagnostic foundation model dataset. (b) Our dataset statistic. (c) Standard planes. The view images are sourced from [21].

diagnostic foundation models with better probe guidance capability at a low training cost.

II. RELATED WORK

A. AI-assisted Ultrasound Scanning

Ultrasound scanning, especially cardiac ultrasound, heavily relies on the operator’s skill and experience. With advancements in AI technology, researchers have begun exploring ways to leverage AI to assist ultrasound scanning, aiming to reduce reliance on operator experience and improve image quality. Amadou et al. [1] relied on cardiac CT scans for simulation and use reinforcement learning to train optimal strategies. However, CT data is costly, and there are significant differences between CT and ultrasound images, limiting its applicability. Hao et al. [9] conduct traversal scanning over predefined positional and angular ranges, followed by deep metric learning to identify target cardiac views from the captured video. However, the approach is relatively slow and may not generalize well across diverse subjects. Bao et al. [3] developed a visual navigation system to assist in locating A4C and A2C views. While useful, it only covers a small subset of the necessary scanning planes, limiting its clinical value. Yue et al. [30] proposed EchoWorld, a motion-aware world modeling framework that pre-trains a cardiac world model to improve probe guidance. However, its training cost is high, and it fails to leverage the rich ultrasound imaging knowledge already embedded in existing ultrasound foundation models.

B. Ultrasound Diagnostic Foundation Model

One major bottleneck in the field of AI-assisted probe navigation is the difficulty of expert demonstration data acquisition. In contrast, AI-driven ultrasound diagnosis benefit from richer data sources, accelerating model development and yielding numerous representative architectures. For example, EchoCLIP [6] is a vision-language model trained on over one million cardiac ultrasound videos paired with expert reports. It shows strong performance across various cardiac diagnostic tasks. USFM [17] is a general-purpose ultrasound model pre-trained on more than two million images from 12 organs. It introduces spatial-frequency masking techniques to handle low-quality images and supports diverse tasks like segmentation and classification. BiomedCLIP [32] is a multimodal model trained on 15 million biomedical image–text pairs. It

achieves state-of-the-art results across retrieval, classification, and visual question answering. While these models were not originally designed for probe guidance, their core capability in ultrasound image interpretation directly addresses a fundamental requirement of probe guidance tasks. Therefore, in this paper, we explore leveraging the knowledge embedded in existing foundation models to enhance probe guidance.

C. Parameter-efficient Fine-tuning

To effectively transfer knowledge from the ultrasound foundation model to the probe guidance task, we employ a parameter-efficient fine-tuning (PEFT) strategy, which preserves the pretrained model’s learned representations while minimizing data and computational requirements. Prominent PEFT strategies include adapters [11], which insert small trainable networks between layers of a frozen model, updating only these adapters for efficient task-specific adaptation. Another popular PEFT method is prefix tuning [19], which keeps the model frozen and learns a small task-specific vector (prefix) added to the self-attention layers to guide model behavior. Besides, Low-Rank Adaptation (LoRA) [12] introduces trainable low-rank matrices into Transformer layers while keeping pre-trained weights frozen, enabling efficient adaptation with few trainable parameters. In this work, we adopt the adapter structure due to its greater flexibility, which allows it to be applied to different network architectures, as EchoCLIP and USFM are built on distinct network frameworks.

III. METHOD

In this section, we first describe the cardiac ultrasound scanning dataset to provide a background about our task. Next, we introduce our vision-action adapter, which equips ultrasound foundation models with the ability to reason about probe adjustment actions for navigating toward target planes.

A. Dataset Acquisition

The dataset used in our work was collected from 178 adult subjects and includes 356 expert scanning trajectories, totaling 1.31 million image-action pairs. The data was gathered by two senior sonographers with over 10 years of experience. They performed continuous scans of 10 standard echocardiographic planes (Fig. 1(c)) using an ultrasound probe attached to the end of a robotic arm. The data collection system recorded real-time

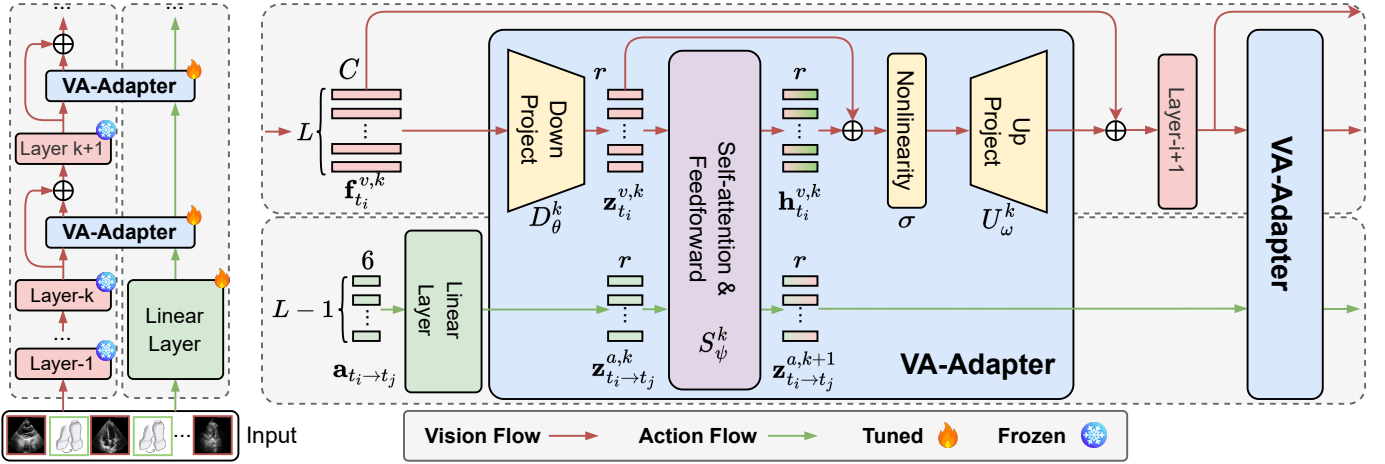


Fig. 2: Illustration of the architecture of the VA-Adapter. The left side shows that we insert VA-Adapter into the deep layers of foundation models, and the right side shows the internal structure of VA-Adapter.

images acquired by the probe and the corresponding probe pose data. This created a scanning sequence $\{(\mathbf{I}_t, \mathbf{p}_t)\}_{t=1}^T$, where $\mathbf{I}_t \in \mathbb{R}^{3 \times H \times W}$ is the ultrasound image at time t , and $\mathbf{p}_t \in \text{SE}(3)$ is the corresponding probe's 6D pose (3D position $\mathbf{P} \in \mathbb{R}^3$ and 3D orientation $\mathbf{R} \in \text{SO}(3)$).

During the scan, the sonographer marked the standard views. Then we can calculate the relative motion of any image \mathbf{I}_i to the standard view \mathbf{I}_j : $\mathbf{a}_{i \rightarrow j} = \mathbf{T}_{p_i}^{-1} \mathbf{T}_{p_j}$, where \mathbf{T}_{p_i} and \mathbf{T}_{p_j} represent the transformation matrices corresponding to the probe poses \mathbf{p}_i and \mathbf{p}_j . Then we use this motion value as the supervisory signal for the ultrasound probe guidance task.

Notably, during data acquisition, the sonographer would sometimes pause scanning at certain probe positions in order to closely observe the dynamic characteristics of the heart. As a result, the dataset contains many images captured from the same probe position but at different phases of the cardiac cycle. These images share the same motion label, which provides a form of implicit supervision that encourages the model to be robust to cardiac cycle variation.

B. Vision-Action Adapter

Echocardiography probe guidance is an emerging research direction. While AI-driven probe guidance systems hold promise for improving echocardiography accessibility, progress has been slow due to the challenges of data collection. In contrast, significant advancements have been made in ultrasound image understanding and diagnosis, with recent foundation models [6], [8], [17], [24] demonstrating exceptional performance on baseline tasks. Notably, a probe guidance model shares the same fundamental ability as these models: understanding structural information in ultrasound images. Thus, we proposed the Vision-Action Adapter to explore the potential of leveraging these foundation models for probe guidance tasks. In the following sections, we will provide a detailed explanation of our approach, as shown in Fig. 2.

Input. First, for a given image $\mathbf{I}_t \in \mathbb{R}^{3 \times H \times W}$ from a particular scan, we segmentally sample $L - 1$ images along with

their corresponding poses from the same scan. The sampling strategy is following [27]. Specifically, we do not use L consecutive frames as the input sequence. Instead, we divide the full scan from a single subject into $L - 1$ equal-length temporal segments, and randomly sample one frame from each segment. These $L - 1$ frames are then sorted in ascending order by their timestamps and combined with the current frame \mathbf{I}_t , which is placed at the end of the sequence as \mathbf{I}_{t_L} . This sampling strategy encourages the model to learn more diverse spatial structural cues by introducing greater variability in anatomy and motion across frames. In contrast, using L adjacent frames would lead to minimal visual and positional differences between input images, making it difficult for the model to capture the full 3D cardiac structure. For reference, in the sequences constructed using our segmental sampling, the average absolute relative motion between adjacent frames is approximately $[21.8 \text{ mm}, 18.7 \text{ mm}, 14.0 \text{ mm}, 12.6^\circ, 23.3^\circ, 40.9^\circ]$, indicating substantial variation in both position and orientation. Next, the relative movement actions $\mathbf{a}_{t_i \rightarrow t_j} \in \mathbb{R}^6$ are computed using their poses, thereby forming a scanning trajectory:

$$[\mathbf{I}_{t_1}, \mathbf{a}_{t_1 \rightarrow t_2}, \dots, \mathbf{I}_{t_{L-1}}, \mathbf{a}_{t_{L-1} \rightarrow t_L}, \mathbf{I}_{t_L}]. \quad (1)$$

Forward propagation. The VA-Adapters are inserted into the latter part of the foundation model's vision encoder, as features in this section are more task-relevant [29]. For convolutional vision encoders (e.g., EchoCLIP), the VA-Adapters are inserted between the blocks in the latter half of the encoder. For transformer-based vision encoders (e.g., USFM and BiomedCLIP), two VA-Adapters are inserted within a Transformer block: one is placed after the attention module, and the other after the MLP module. Only the VA-Adapters are trained, while the foundation model remains frozen to preserve its learned knowledge. We assume that after passing through the initial k -th vision layers, the image \mathbf{I}_{t_i} yields feature $\mathbf{f}_{t_i}^{v,k} \in \mathbb{R}^C$. Note that for a convolutional vision encoder, we apply global average pooling to convert the feature map into a vector feature. Then, visual features are input into the VA-

Adapter, first passing through a down projection layer D_θ^k , while raw actions are transformed by a linear layer A_ϕ^k to align their dimensions:

$$\begin{aligned} \mathbf{z}_{t_i}^{v,k} &= D_\theta^k(\mathbf{f}_{t_i}^{v,k}) + \mathbf{T}_i, \quad \mathbf{z}_{t_i}^{v,k} \in \mathbb{R}^r \\ \mathbf{z}_{t_i \rightarrow t_j}^{a,k} &= A_\phi^k(\mathbf{a}_{t_i \rightarrow t_j}) + \mathbf{T}_i, \quad \mathbf{z}_{t_i \rightarrow t_j}^{a,k} \in \mathbb{R}^r \end{aligned} \quad (2)$$

where $\mathbf{T} \in \mathbb{R}^{L \times r}$ is timestep embedding, and r represents the bottleneck dimension of the VA-Adapter. Furthermore, this image and action sequence is fed into a vision-action interaction module S_ψ^k , designed to extract underlying cardiac structure information:

$$[\mathbf{h}_{t_1}^{v,k}, \mathbf{z}_{t_1 \rightarrow t_2}^{a,k+1}, \dots, \mathbf{h}_{t_L}^{v,k}] = S_\psi^k([\mathbf{z}_{t_1}^{v,k}, \mathbf{z}_{t_1 \rightarrow t_2}^{a,k}, \dots, \mathbf{z}_{t_{L-1}}^{v,k}, \mathbf{z}_{t_{L-1} \rightarrow t_L}^{a,k}, \mathbf{z}_{t_L}^{v,k}]). \quad (3)$$

The action features $\mathbf{z}_{t_i \rightarrow t_j}^{a,k+1}$ are directly input into the next layer of the VA-Adapter. The visual features $\mathbf{h}_{t_i}^{v,k}$ are further processed through a nonlinear layer σ and an up projection layer U_ω^j to generate the VA-Adapter's output:

$$\mathbf{z}_{t_i}^{v,k+1} = U_\omega^k(\sigma(\mathbf{h}_{t_i}^{v,k} + \mathbf{z}_{t_i}^{v,k})) + \mathbf{f}_{t_i}^{v,k}, \quad (4)$$

C. Task Prediction Head

After passing through all layers (assuming the network has M layers in total), we obtain the following sequence features:

$$[\mathbf{z}_{t_1}^{v,M}, \mathbf{z}_{t_1 \rightarrow t_2}^{a,M}, \dots, \mathbf{z}_{t_{L-1}}^{v,M}, \mathbf{z}_{t_{L-1} \rightarrow t_L}^{a,M}, \mathbf{z}_{t_L}^{v,M}]. \quad (5)$$

The objective of our probe movement guidance task is to predict the relative movement action from any given plane to the ten standard planes. Thus, we introduce ten prediction heads H_{ξ_i} , $i \in \mathbb{Z}$, $1 \leq i \leq 10$ to predict the action toward each standard plane. Formally, the forward process for predicting action from I_{t_L} to i -th standard plane can be represented as:

$$\mathbf{m}^a = E_\rho([\mathbf{z}_{t_1}^{v,M}, \mathbf{z}_{t_1 \rightarrow t_2}^{a,M}, \dots, \mathbf{z}_{t_{L-1}}^{v,M}, \mathbf{z}_{t_{L-1} \rightarrow t_L}^{a,M}, \mathbf{z}_{t_L}^{v,M}, \mathbf{m}^a]), \quad (6)$$

$$\mathbf{a}'_{t_L \rightarrow t_{i\text{-th standard plane}}} = H_{\xi_i}(\mathbf{m}^a), \quad (7)$$

where \mathbf{m}^a represents a global sequence token, and E_ρ is sequence encoder implemented as a GRU to further integrate the information within the sequence.

Finally, the loss is calculated using the Smooth L1 Loss between the predicted action and the target $\mathbf{a}_{t_L \rightarrow t_{i\text{-th standard plane}}}$ as follows:

$$\mathcal{L} = \mathcal{L}_{\text{SmoothL1}}(\mathbf{a}_{t_L \rightarrow t_{i\text{-th standard plane}}}, \mathbf{a}'_{t_L \rightarrow t_{i\text{-th standard plane}}}). \quad (8)$$

In (8), translation and rotation are treated with equal weight in the loss computation, which aligns with the fact that both dimensions are equally important in cardiac ultrasound scanning. Additionally, to prevent the model from being biased toward one dimension due to significant numerical disparities, we adjusted the units during preprocessing (millimeter for translation and degree for rotation) to ensure their values fall within the same order of magnitude.

A. Datasets and Implementation Details

a) *Datasets*: Data were collected using a GE machine equipped with an M5S probe, and the collection method is described in Section III-A. The entire data collection process was approved and supervised by the University Medical Ethics Committee. In our experiment, 284 scans were used for training and 72 for validation, with data from different subjects in each set.

b) *Model Architecture*: The length of the input image sequence L is set to 4 by default. The bottleneck dimension r (adapter dimension) in our VA-Adapter is set to 64 by default. The activation function uses ReLU. The core vision-action interaction module S_ψ is implemented as a Transformer block that employs 4 attention heads and an MLP ratio of 2, meaning that the hidden dimension of the feed-forward layers is twice the embedding dimension. The positional encoding of the vision-action features employs a 1-dimensional sincos encoding method. The weights of fully connected layers and convolutional layers are initialized using a truncated normal distribution, with biases initialized to 0 and variance set to 0.02. The weights of layer normalization are initialized to 1 and biases to 0. After passing through the image encoder, the image features and action features are mapped to a dimension of 128 through the linear layer respectively, and then concatenated before being input to the sequence encoder E_ρ , which is a GRU with an input dimension of 256 and a hidden layer dimension of 128. The final prediction head H_{ξ_i} consists of two MLP layers, with a GELU activation function applied between them.

c) *Training Strategy*: During training, the Adam optimizer is used with a batch size of 256, an initial learning rate of 1×10^{-4} , and a cosine learning rate decay strategy, with a final learning rate of 1×10^{-6} . Training runs for 5 epochs, and all experiments are performed on four A100 GPUs.

d) *Evaluation Metric*: We use two evaluation metrics to assess performance: the training parameter count and the mean absolute error (MAE) between the predicted action \mathbf{a}' and the ground-truth \mathbf{a} . The MAE is computed separately for the translation and rotation:

$$\text{MAE of Translation} = \frac{1}{3} \sum_{i=1}^3 |\mathbf{a}_i - \mathbf{a}'_i|, \quad (9)$$

$$\text{MAE of Rotation} = \frac{1}{3} \sum_{i=4}^6 |\mathbf{a}_i - \mathbf{a}'_i|. \quad (10)$$

B. Comparison with Baselines

We evaluated our method on ten standard views, as shown in Table I and Table II. Our method outperforms baselines in both MAE and parameter efficiency. Single-frame input models make decisions based only on the current image, failing to model variations in cardiac structure, leading to poor performance. Baseline sequential models [4], [7] typically fuse image and action features only in the task prediction head after

TABLE I: **Comparison with baseline methods in the translation dimension.** † indicates that these methods use the pre-trained encoder from DeiT. Plane numbers correspond to Fig. 1(c).

Method	Trained Params	MAE of the translation dimension for the ten standard planes (mm)										Avg.
		1	2	3	4	5	6	7	8	9	10	
<i>Single-frame, pre-trained on ImageNet</i>												
DeiT [26]	22.60M	8.50	8.09	8.51	7.90	7.85	9.21	8.43	8.55	8.70	8.52	8.43
DINOv2 [23]	90.28M	8.31	7.82	8.36	7.70	7.66	9.09	8.40	8.52	8.70	8.62	8.22
<i>Single-frame, pre-trained on ultrasound data</i>												
BiomedCLIP [32]	89.50M	8.40	7.89	8.44	7.79	7.78	9.16	8.62	8.73	8.88	8.75	8.44
LVM-Med [20]	89.44M	8.55	8.00	8.42	7.95	7.89	9.31	8.70	8.88	9.07	8.80	8.56
US-MoCo [5]	22.60M	8.75	8.08	8.29	7.95	7.90	9.22	8.55	8.78	8.88	8.74	8.51
US-IJEPa [2]	22.59M	8.28	7.82	8.36	7.74	7.74	8.84	8.46	8.55	9.01	8.67	8.35
US-MAE [10]	22.60M	8.31	7.74	8.30	7.69	7.70	9.02	8.35	8.47	8.55	8.45	8.26
USFM [17]	92.94M	8.34	7.74	8.28	7.62	7.69	9.02	8.20	8.33	8.51	8.39	8.26
EchoCLIP [6]	89.74M	8.29	7.78	8.45	7.53	7.60	9.17	8.16	8.22	8.58	8.35	8.21
<i>Sequential, pre-trained on ImageNet</i>												
US-GuideNet† [7]	22.05M	6.81	7.59	8.63	6.70	7.05	8.09	7.28	7.28	8.05	7.84	7.53
Decision-T† [4]	22.27M	6.69	7.60	8.46	6.71	6.81	7.87	7.01	7.06	7.92	7.67	7.38
<i>Sequential, pre-trained on ultrasound data</i>												
BiomedCLIP	86.15M	6.87	6.67	7.26	6.32	6.31	8.09	7.77	7.87	7.95	7.83	7.29
BiomedCLIP+ours	3.94M	6.12	5.78	6.28	5.25	5.18	6.65	5.03	4.97	5.30	4.94	5.55
USFM	87.04M	6.48	6.34	6.84	6.05	5.93	7.72	8.07	8.16	8.05	7.86	7.15
USFM+ours	3.97M	6.04	5.40	5.40	5.20	5.01	6.72	4.94	5.13	5.07	4.60	5.35
EchoCLIP	88.41M	6.31	6.03	6.48	5.76	5.76	7.31	7.03	7.05	6.96	6.95	6.56
EchoCLIP+ours	2.61M	5.94	5.55	6.03	5.17	4.99	6.90	4.77	4.87	5.11	4.63	5.40

TABLE II: **Comparison with baseline methods in the rotation dimension.** † indicates that these methods use the pre-trained encoder from DeiT. Plane numbers correspond to Fig. 1(c).

Method	Trained Params	MAE of the rotation dimension for the ten standard planes (°)										Avg.
		1	2	3	4	5	6	7	8	9	10	
<i>Single-frame, pre-trained on ImageNet</i>												
DeiT [26]	22.60M	7.27	8.02	8.71	8.66	8.62	9.23	7.37	9.54	9.71	11.28	8.84
DINOv2 [23]	90.28M	7.21	7.82	8.75	8.66	8.42	9.04	7.27	9.41	9.38	11.27	8.72
<i>Single-frame, pre-trained on ultrasound data</i>												
BiomedCLIP [32]	89.50M	7.33	8.00	8.84	8.88	8.85	9.38	7.81	10.04	9.59	11.62	9.03
LVM-Med [20]	89.44M	7.26	7.94	8.62	8.81	8.85	9.27	7.59	9.65	9.65	11.34	8.90
US-MoCo [5]	22.60M	7.46	7.90	8.64	8.76	8.64	9.23	7.40	9.76	9.70	11.55	8.80
US-IJEPa [2]	22.59M	7.24	7.75	7.98	8.73	8.46	9.06	7.57	9.72	9.42	10.81	8.67
US-MAE [10]	22.60M	7.11	7.61	8.23	8.55	8.56	9.05	7.26	9.67	9.46	11.05	8.66
USFM [17]	92.94M	7.14	7.69	8.51	8.38	8.41	9.00	7.18	9.38	9.37	11.14	8.62
EchoCLIP [6]	89.74M	6.86	7.52	8.51	8.44	8.47	9.18	7.03	9.31	8.88	10.97	8.52
<i>Sequential, pre-trained on ImageNet</i>												
US-GuideNet† [7]	22.05M	5.88	7.21	7.22	8.00	7.88	8.52	6.68	7.39	8.39	11.13	7.83
Decision-T† [4]	22.27M	5.94	7.38	7.30	8.27	8.20	8.70	6.48	7.41	8.18	10.89	7.88
<i>Sequential, pre-trained on ultrasound data</i>												
BiomedCLIP	86.15M	6.17	6.62	7.05	7.73	7.58	7.90	6.72	9.32	8.43	10.46	7.80
BiomedCLIP+ours	3.94M	5.55	5.65	5.90	5.83	5.32	6.58	5.76	8.08	8.51	9.75	6.69
USFM	87.04M	6.34	6.67	6.92	7.05	6.79	7.95	6.90	9.56	9.07	10.82	7.81
USFM+ours	3.97M	5.47	6.17	6.18	5.28	4.82	6.67	5.70	8.06	8.56	10.18	6.71
EchoCLIP	88.41M	6.00	6.69	7.20	6.87	6.75	7.51	6.65	8.99	9.06	10.91	7.66
EchoCLIP+ours	2.61M	5.36	5.93	5.98	5.62	5.30	6.59	5.83	8.19	8.42	10.17	6.74

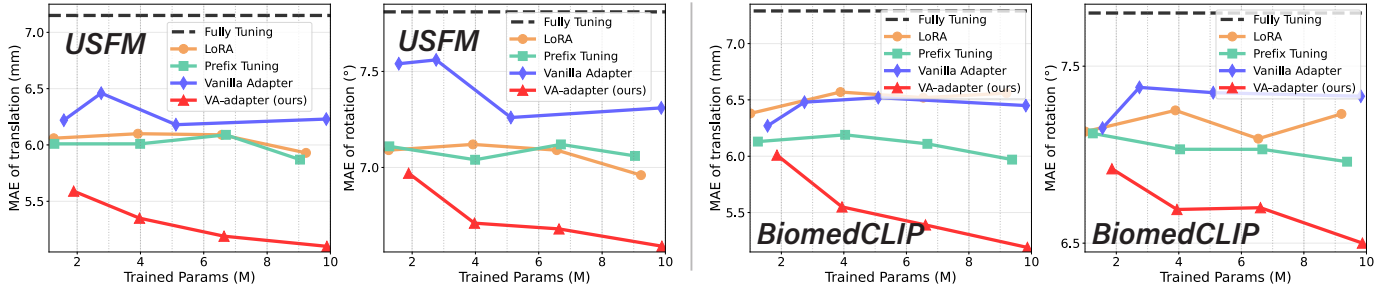


Fig. 3: Performance comparison of different PEFT methods on USFM and BiomedCLIP.

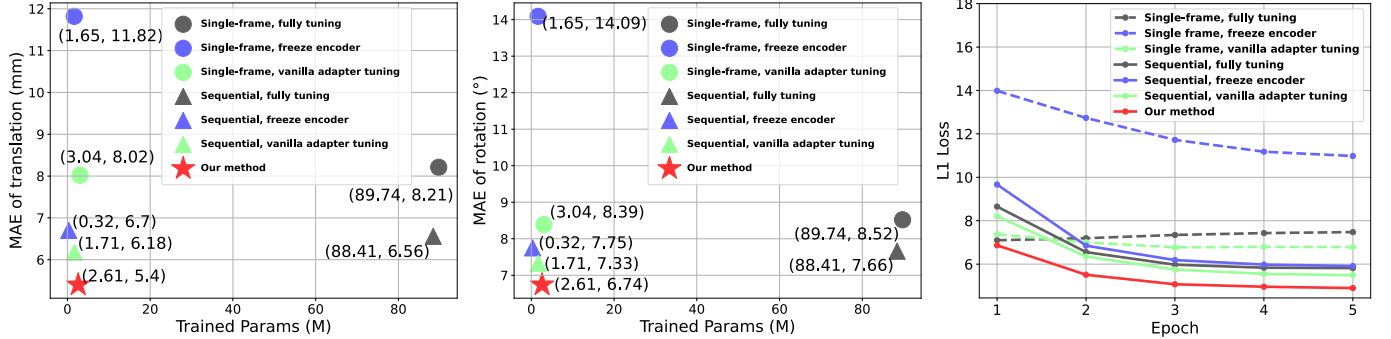


Fig. 4: Ablation study on vision-action interaction module of the EchoCLIP model.

the encoder, failing to fully leverage the individual cardiac structure information embedded in the sequence. Additionally, due to full-scale fine-tuning, these methods incur high training costs. Our approach inserts a lightweight VA-Adapter into the image encoder, enabling the model to gradually learn cardiac structural features during the feature extraction phase, optimizing both efficiency and performance at the same time.

We also compared our method with other common PEFT methods, including LoRA [12] and Prefix Tuning [19]. As these methods were originally designed for transformer-based models, we only conducted experiments on the transformer-based USFM and BiomedCLIP. As shown in Fig. 3, our VA-Adapter achieves the best performance. One key reason is that we introduce a sequence modeling paradigm—our VA-Adapter enables interaction between visual and action features, allowing the model to better understand cardiac structures. In contrast, other PEFT methods mainly reduce training cost and overfitting risk, but do not enhance the model’s capacity to understand cardiac structures, which limits their performance on our task.

C. Ablation Study

a) *Vision-action Interaction Module:* We performed a comparative analysis of seven training baselines for the EchoCLIP model, as shown in Fig. 4. The vanilla adapter tuning removes the vision-action interaction module from the VA-Adapter, with all other settings identical to ours. Our approach, with 2.61M parameters, achieves the lowest MAE, showing a significant advantage in parameter efficiency. Even compared to the vanilla adapter method with a similar parameter size, our approach reduces the MAE by 12.6% / 8.0% (Trans. / Rot.) with only an additional 0.9M parameters, demonstrating

that the performance gains from the vision-action interaction mechanism outweigh the marginal cost of extra parameters. Our method achieves the optimal trade-off between training parameter count and MAE. Furthermore, it also demonstrates faster convergence, surpassing other methods by the end of the first epoch.

b) *Adapter Dimension:* We analyzed the impact of different adapter dimension on model performance and training parameters. The experimental results, as shown in Fig. 5, thoroughly validate the effectiveness and parameter efficiency of our proposed method. When adapter dimension is equal to 8, our method introduces only 0.2M parameters (0.23% of the fully tuning encoder parameters), reducing the MAE by 11.9% / 8.2% (Trans. / Rot.), while the vanilla Adapter, with nearly the same number of parameters, only achieves a 4.6% / 4.2% (Trans. / Rot.) reduction. This demonstrates that the adapter proposed in this paper can efficiently capture the spatial structural characteristics of the heart with a minimal number of parameters, addressing the issue of significant information loss in low-dimensional spaces typical of traditional Adapters.

Furthermore, when the adapter dimension of our method increases from 8 to 128, the parameter count grows by 31.7× while the MAE decreases by 9.2% / 6.3% (Trans. / Rot.). In contrast, for the vanilla adapter, the parameter count increases by 15.4× with only a 0.2% / 2.0% (Trans. / Rot.) MAE reduction. This proves that our interaction module enables more effective parameter utilization, with each additional parameter contributing to a larger performance gain.

D. Visualization

Finally, we visualized the model’s output, as shown in Fig. 6. Based on the action predicted by the model, we

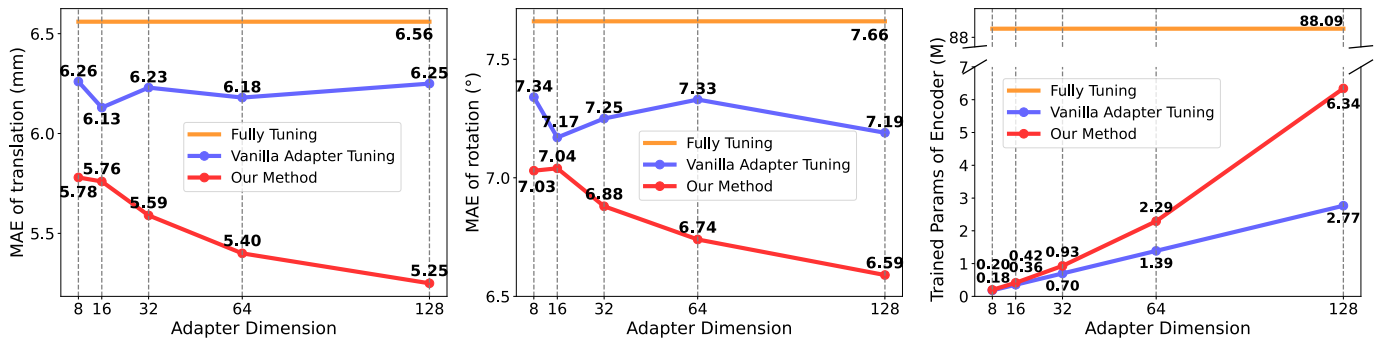


Fig. 5: Ablation study on adapter dimension of the EchoCLIP model.

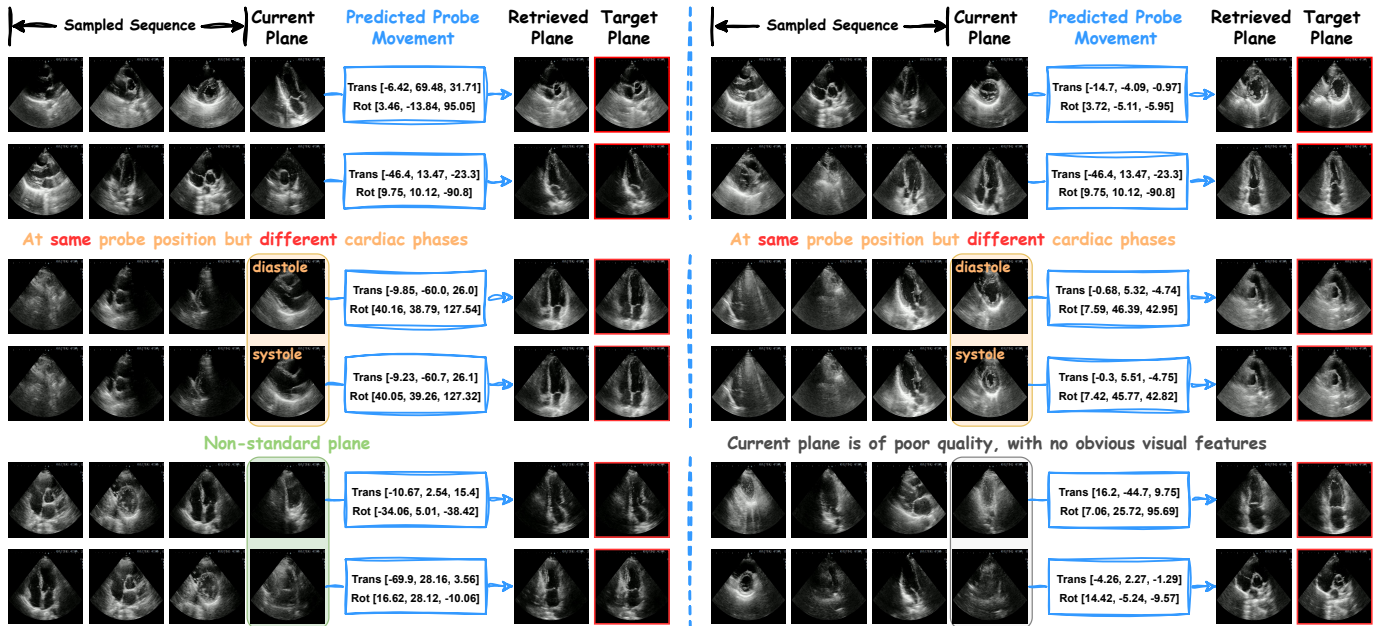


Fig. 6: Visualization of the model's prediction.

computed the posture achieved after executing the action. We then performed nearest-neighbor retrieval in the scan sequence based on this posture, comparing the retrieved plane with the target plane. The results show that the model successfully guides the probe to the target plane. Furthermore, it can be observed that the model outputs remain consistent for images from the same probe position but at different cardiac phases, indicating robustness to the cardiac cycle. In addition, for non-standard planes or planes of very poor quality with no obvious visual features, our sequence model is still able to infer the correct decision based on the relationships between images and actions in the input sequence. This capability is not attainable with single-frame models.

E. Inference Real-time Analysis

We evaluated the real-time inference performance of our model on two different GPUs: A100 and RTX 3090. As shown in Table III, the inference time for a single input sequence is approximately 10 milliseconds on both devices, which fully meets the requirements for real-time performance in clinical applications. Moreover, it can be observed that the introduction

TABLE III: Inference real-time analysis. We show the inference time for one sequence on various GPU devices.

Method	RTX3090	A100
BiomedCLIP	10.020 ms	8.464 ms
BiomedCLIP + VA-Adapter	10.548 ms	8.964 ms
USFM	10.680 ms	9.380 ms
USFM + VA-Adapter	11.240 ms	9.804 ms
EchoCLIP	11.104 ms	9.476 ms
EchoCLIP + VA-Adapter	11.828 ms	9.700 ms

of the VA-Adapter has a negligible impact on inference speed. This demonstrates that our method not only achieves high accuracy but also maintains excellent computational efficiency, making it suitable for deployment in time-sensitive ultrasound guidance scenarios.

V. CONCLUSION

In this paper, we propose VA-Adapter, a lightweight module that empowers ultrasound diagnostic foundation models with

probe guidance capability by modeling vision-action interactions during feature encoding. By combining basic knowledge from the ultrasound foundation model with personalized 3D cardiac structures learned from the VA-Adapter, our model achieves excellent probe guidance performance. Compared to fully fine-tuning methods, our approach reduces the training parameter count by 95.4%–97.0% and decreases guidance error by 12.0%–25.2%. Extensive experiments further validate the higher parameter efficiency and better guidance performance of our method compared with state-of-the-art baselines.

REFERENCES

- [1] Amadou, A.A., Singh, V., Ghesu, F.C., Kim, Y.H., Stanculescu, L., Sai, H.P., Sharma, P., Young, A., Rajani, R., Rhode, K.: Goal-conditioned reinforcement learning for ultrasound navigation guidance. arXiv preprint arXiv:2405.01409 (2024)
- [2] Assran, M., Duval, Q., Misra, I., Bojanowski, P., Vincent, P., Rabat, M., LeCun, Y., Ballas, N.: Self-supervised learning from images with a joint-embedding predictive architecture. In: Proceedings of the IEEE/CVF Conference on Computer Vision and Pattern Recognition. pp. 15619–15629 (2023)
- [3] Bao, M., Wang, Y., Wei, X., Jia, B., Fan, X., Lu, D., Gu, Y., Cheng, J., Zhang, Y., Wang, C., et al.: Real-world visual navigation for cardiac ultrasound view planning. In: International Conference on Medical Image Computing and Computer-Assisted Intervention. pp. 317–326. Springer (2024)
- [4] Chen, L., Lu, K., Rajeswaran, A., Lee, K., Grover, A., Laskin, M., Abbeel, P., Srinivas, A., Mordatch, I.: Decision transformer: Reinforcement learning via sequence modeling. *Advances in neural information processing systems* **34**, 15084–15097 (2021)
- [5] Chen, X., Xie, S., He, K.: An empirical study of training self-supervised vision transformers. In: Proceedings of the IEEE/CVF international conference on computer vision. pp. 9640–9649 (2021)
- [6] Christensen, M., Vukadinovic, M., Yuan, N., Ouyang, D.: Vision-language foundation model for echocardiogram interpretation. *Nature Medicine* pp. 1–8 (2024)
- [7] Droste, R., Drukker, L., Papageorghiou, A.T., Noble, J.A.: Automatic probe movement guidance for freehand obstetric ultrasound. In: Medical Image Computing and Computer Assisted Intervention—MICCAI 2020: 23rd International Conference, Lima, Peru, October 4–8, 2020, Proceedings, Part III 23. pp. 583–592. Springer (2020)
- [8] Ghorbani, A., Ouyang, D., Abid, A., He, B., Chen, J.H., Harrington, R.A., Liang, D.H., Ashley, E.A., Zou, J.Y.: Deep learning interpretation of echocardiograms. *NPJ digital medicine* **3**(1), 10 (2020)
- [9] Hao, M., Zhang, P., Hou, X., Gu, X., Zhou, X.H., Hou, Z.G., Chen, C., Wang, S.: Towards autonomous cardiac ultrasound scanning: Combining physician expertise and machine intelligence. *IEEE Transactions on Medical Robotics and Bionics* **7**(2), 782–792 (2025)
- [10] He, K., Chen, X., Xie, S., Li, Y., Dollár, P., Girshick, R.: Masked autoencoders are scalable vision learners. In: Proceedings of the IEEE/CVF conference on computer vision and pattern recognition. pp. 16000–16009 (2022)
- [11] Houlsby, N., Giurgiu, A., Jastrzebski, S., Morrone, B., De Laroussilhe, Q., Gesmundo, A., Attariyan, M., Gelly, S.: Parameter-efficient transfer learning for NLP. In: Proceedings of the 36th International Conference on Machine Learning. pp. 2790–2799 (2019)
- [12] Hu, E.J., Shen, Y., Wallis, P., Allen-Zhu, Z., Li, Y., Wang, S., Chen, W.: Lora: Low-rank adaptation of large language models. *CoRR abs/2106.09685* (2021)
- [13] Jiang, H., Li, M., Sun, Z., Jia, N., Sun, Y., Luo, S., Song, S., Huang, G.: Structure-aware world model for probe guidance via large-scale self-supervised pre-train. In: International Workshop on Advances in Simplifying Medical Ultrasound. pp. 58–67. Springer (2024)
- [14] Jiang, H., Sun, Z., Jia, N., Li, M., Sun, Y., Luo, S., Song, S., Huang, G.: Cardiac copilot: Automatic probe guidance for echocardiography with world model. In: International Conference on Medical Image Computing and Computer-Assisted Intervention. pp. 190–199. Springer (2024)
- [15] Jiang, H., Sun, Z., Sun, Y., Jia, N., Li, M., Luo, S., Song, S., Huang, G.: Sequence-aware pre-training for echocardiography probe guidance. arXiv preprint arXiv:2408.15026 (2024)
- [16] Jiang, H., Zhao, A., Yang, Q., Yan, X., Wang, T., Wang, Y., Jia, N., Wang, J., Wu, G., Yue, Y., et al.: Towards expert-level autonomous carotid ultrasonography with large-scale learning-based robotic system. *Nature Communications* **16**(1), 7893 (2025)
- [17] Jiao, J., Zhou, J., Li, X., Xia, M., Huang, Y., Huang, L., Wang, N., Zhang, X., Zhou, S., Wang, Y., et al.: Usfm: A universal ultrasound foundation model generalized to tasks and organs towards label efficient image analysis. *Medical Image Analysis* **96**, 103202 (2024)
- [18] Li, K., Li, A., Xu, Y., Xiong, H., Meng, M.Q.H.: RI-tee: Autonomous probe guidance for transesophageal echocardiography based on attention-augmented deep reinforcement learning. *IEEE Transactions on Automation Science and Engineering* **21**(2), 1526–1538 (2023)
- [19] Li, X.L., Liang, P.: Prefix-tuning: Optimizing continuous prompts for generation. In: Proceedings of the 59th Annual Meeting of the Association for Computational Linguistics and the 11th International Joint Conference on Natural Language Processing (Volume 1: Long Papers) (2021)
- [20] MH Nguyen, D., Nguyen, H., Diep, N., Pham, T.N., Cao, T., Nguyen, B., Swoboda, P., Ho, N., Albarqouni, S., Xie, P., et al.: Lvm-med: Learning large-scale self-supervised vision models for medical imaging via second-order graph matching. *Advances in Neural Information Processing Systems* **36** (2024)
- [21] Mitchell, C., Rahko, P.S., Blauwet, L.A., Canaday, B., Finstuen, J.A., Foster, M.C., Horton, K., Ogunyankin, K.O., Palma, R.A., Velazquez, E.J.: Guidelines for performing a comprehensive transthoracic echocardiographic examination in adults: recommendations from the american society of echocardiography. *Journal of the American Society of Echocardiography* **32**(1), 1–64 (2019)
- [22] Narang, A., Bae, R., Hong, H., Thomas, Y., Surette, S., Cadieu, C., Chaudhry, A., Martin, R.P., McCarthy, P.M., Rubenson, D.S., et al.: Utility of a deep-learning algorithm to guide novices to acquire echocardiograms for limited diagnostic use. *JAMA cardiology* **6**(6), 624–632 (2021)
- [23] Oquab, M., Darcet, T., Moutakanni, T., Vo, H., Szafraniec, M., Khalidov, V., Fernandez, P., Haziza, D., Massa, F., El-Nouby, A., et al.: Dinov2: Learning robust visual features without supervision. arXiv preprint arXiv:2304.07193 (2023)
- [24] Ouyang, D., He, B., Ghorbani, A., Yuan, N., Ebinger, J., Langlotz, C.P., Heidenreich, P.A., Harrington, R.A., Liang, D.H., Ashley, E.A., et al.: Video-based ai for beat-to-beat assessment of cardiac function. *Nature* **580**(7802), 252–256 (2020)
- [25] Roth, G.A., Johnson, C., Abajobir, A., Abd-Allah, F., Abera, S.F., Abyu, G., Ahmed, M., Aksut, B., Alam, T., Alam, K., et al.: Global, regional, and national burden of cardiovascular diseases for 10 causes, 1990 to 2015. *Journal of the American college of cardiology* **70**(1), 1–25 (2017)
- [26] Touvron, H., Cord, M., Douze, M., Massa, F., Sablayrolles, A., Jégou, H.: Training data-efficient image transformers & distillation through attention. In: International conference on machine learning. pp. 10347–10357. PMLR (2021)
- [27] Wang, L., Xiong, Y., Wang, Z., Qiao, Y., Lin, D., Tang, X., Van Gool, L.: Temporal segment networks: Towards good practices for deep action recognition. In: European conference on computer vision. pp. 20–36. Springer (2016)
- [28] Wang, T., Jiang, H., Wang, Y., Sun, Z., Yan, X., Li, X., Huang, G.: Ultrahit: A hierarchical transformer architecture for generalizable internal carotid artery robotic ultrasonography. arXiv preprint arXiv:2509.13832 (2025)
- [29] Yang, L., Zhang, R.Y., Wang, Y., Xie, X.: Mma: Multi-modal adapter for vision-language models. In: Proceedings of the IEEE/CVF Conference on Computer Vision and Pattern Recognition. pp. 23826–23837 (2024)
- [30] Yue, Y., Wang, Y., Jiang, H., Liu, P., Song, S., Huang, G.: Echoworld: Learning motion-aware world models for echocardiography probe guidance. In: Proceedings of the Computer Vision and Pattern Recognition Conference. pp. 25993–26003 (2025)
- [31] Yue, Y., Wang, Y., Tao, C., Liu, P., Song, S., Huang, G.: Chexworld: Exploring image world modeling for radiograph representation learning. In: Proceedings of the Computer Vision and Pattern Recognition Conference. pp. 20778–20788 (2025)
- [32] Zhang, S., Xu, Y., Usuyama, N., Xu, H., Bagga, J., Tinn, R., Preston, S., Rao, R., Wei, M., Valluri, N., et al.: Biomedclip: a multimodal biomedical foundation model pretrained from fifteen million scientific image-text pairs. arXiv preprint arXiv:2303.00915 (2023)